DEUTSCHES ELEKTRONEN-SYNCHROTRON **DESY**

DESY 80/29
April 1980

TWO-PARTICLE INCLUSIVE DISTRIBUTIONS FROM FIRST-ORDER QCD

by

K. Mursula
II. Institut für Theoretische Physik der Universität Hamburg

NOTKESTRASSE 85 · 2 HAMBURG 52

To be sure that your preprints are promptly included in the
HIGH ENERGY PHYSICS INDEX ,
send them to the following address (if possible by air mail) :

DESY
Bibliothek
Notkestrasse 85
2 Hamburg 52
Germany

DESY 80/29
April 1980

Two-Particle Inclusive Distributions from First-Order QCD

K.Mursula+
II.Institut für Theoretische Physik der Universität
Hamburg,Germany

+) Address after 3o.7.198o: Dept.of Theor.Physics,
Univ.of Oulu, Finland

1. Introduction

The quark-parton model predicts certain quantum number correlations[1] for leading ($x \to 1$) hadrons from the lowest order e^+e^--annihilation diagram (see fig.1a). The hadrons are supposed to traverse into opposite directions, excluding a small non-perturbative transverse momentum.

Since lately there is evidence [2] for non-symmetrical jet spread, which is nicely explained by first-order perturbative QCD to be due to gluon bremsstrahlung (see fig.1b and c). An infrared finite correlation function for charged particles in opposite hemispheres has been calculated[3], which directly measures the first-order QCD contribution. Extensive work has been done in order to estimate the other signatures of gluon bremsstrahlung, such as three-jet structure[4], p_T-broadening and "seagull"-effect [5] and topological correlations [6-7].

In this work we study the two-particle correlations of hadrons in opposite hemispheres and with a definite charge from figures 1.b and c. The aim is to extract some knowledge about the properties of the gluon. This calculation is more of an exploratory nature in order to find the kinematic regions where the influence of the emitted gluon is largest. We do not aim to produce results which can directly be compared to experimental data because we neglect the non-perturbative transverse momentum of the emitted particle. Therefore our results become valid only at extremely high energies. At moderate energies, as available now, non-perturbative corrections must be applied as has been done for single particle distributions in ref.8.

The plan of the paper is as follows. In section 2 we give the complete formulas for two-particle distributions including all angular dependences for unpolarized beams. We derive various quantities which show the influence of the gluon. Section 3 contains the results and a comparison with experimental data about two-particle correlations from the Pluto group [9].

2. Two-particle distributions

Neglecting all particle masses and considering only the case of unpolarized lepton beams the differential cross section for the primordial reaction $e^+e^- \to \gamma^* \to q(p_1)\,\bar{q}(p_2)\,g(p_3)$ is given by [6]

$$2\pi \cdot \frac{d^4\sigma}{dz_1\,dz_2\,d\cos\theta\,d\chi} = \frac{3}{8}(1+\cos^2\theta)\cdot\frac{d^2\sigma_U}{dz_1\,dz_2} + \frac{3}{4}\sin^2\theta\,\frac{d^2\sigma_L}{dz_1\,dz_2} + \frac{3}{4}\sin^2\theta\cos 2\chi\,\frac{d^2\sigma_T}{dz_1\,dz_2} - \frac{3}{2\sqrt{2}}\sin 2\theta\cdot\cos\chi\cdot\frac{d^2\sigma_I}{dz_1\,dz_2} \qquad (2.1)$$

where $z_i = 2|\vec{p}_i|/\sqrt{q^2}$, $\sum_i z_i = 2$. θ is the angle between the e^-- beam and the thrust axis (= the most energetic particle) and χ is the azimuthal angle of the $q\bar{q}g$ -production plane relative to the scattering plane (defined by e^--beam and the thrust-axis).

The different contributions to the two-particle inclusive cross section are listed in figure 2. Since we do not consider the non-perturbative p_T - spread of the jets, the topological structure for the hadrons (with respect to θ and χ) remains the same as for the primordial particles. However, we have to define θ and χ with respect to the outcoming hadrons. This we do as follows: θ is now the angle between the e^--beam and hadron h_1. The positive x-axis of the production plane is defined by the other hadron h_2. As the next step we have to calculate the primordial cross sections σ_i in the different cases of figure 2. We introduce the following notation:

σ_i^{rs} ; $r,s = 1,2,3$; $i = U, L, T, I$, which means that the hadron h_1 (resp.h_2) originates from the primordial quantum r (resp. s).

The values 1,2 and 3 of r and s correspond to the quark, antiquark and the gluon, respectively. The different cross sections are:

A. σ_U :

$$\frac{d^2\sigma_U^{12}}{dz_1\,dz_2} = \frac{d^2\sigma_U^{13}}{dz_1\,dz_2} = \sigma^{(1)}\cdot\frac{z_1^2+z_2^2(1-\frac{1}{2}\sin^2\theta_{12})}{(1-z_1)(1-z_2)}$$

$$\frac{d^2\sigma_U^{21}}{dz_1\,dz_2} = \frac{d^2\sigma_U^{23}}{dz_1\,dz_2} = \sigma^{(1)}\cdot\frac{z_2^2+z_1^2(1-\frac{1}{2}\sin^2\theta_{12})}{(1-z_1)(1-z_2)} \qquad (2.2)$$

$$\frac{d^2\sigma_U^{31}}{dz_1\,dz_2} = \frac{d^2\sigma_U^{32}}{dz_1\,dz_2} = \sigma^{(1)}\cdot\frac{z_1^2(1-\frac{1}{2}\sin^2\theta_{13})+z_2^2(1-\frac{1}{2}\sin^2\theta_{23})}{(1-z_1)(1-z_2)}$$

B. σ_L :

$$\frac{d^2\sigma_L^{12}}{dz_1\,dz_2} = \frac{d^2\sigma_L^{13}}{dz_1\,dz_2} = \sigma^{(1)}\cdot\frac{1}{2}\,\frac{z_2^2\sin^2\theta_{12}}{(1-z_1)(1-z_2)}$$

$$\frac{d^2\sigma_L^{21}}{dz_1\,dz_2} = \frac{d^2\sigma_L^{23}}{dz_1\,dz_2} = \sigma^{(1)}\cdot\frac{1}{2}\,\frac{z_1^2\sin^2\theta_{12}}{(1-z_1)(1-z_2)}$$

$$\frac{d^2\sigma_L^{31}}{dz_1\,dz_2} = \frac{d^2\sigma_L^{32}}{dz_1\,dz_2} = \sigma^{(1)}\cdot\frac{1}{2}\,\frac{z_1^2\sin^2\theta_{13}+z_2^2\sin^2\theta_{23}}{(1-z_1)(1-z_2)} \qquad (2.3)$$

C. σ_T :

$$\frac{d^2\sigma_T^{rs}}{dz_1\,dz_2} = \frac{1}{2}\cdot\frac{d^2\sigma_L^{rs}}{dz_1\,dz_2} \quad \text{for all } r,s. \qquad (2.4)$$

D. σ_I :

$$\frac{d^2\sigma_I^{12}}{dz_1\,dz_2} = -\frac{d^2\sigma_I^{13}}{dz_1\,dz_2} = \sigma^{(1)}\cdot\frac{1}{4\sqrt{2}}\cdot\frac{z_2^2\sin 2\theta_{12}}{(1-z_1)(1-z_2)}$$

$$\frac{d^2\sigma_I^{21}}{dz_1\,dz_2} = -\frac{d^2\sigma_I^{23}}{dz_1\,dz_2} = \sigma^{(1)}\cdot\frac{1}{4\sqrt{2}}\cdot\frac{z_1^2\sin 2\theta_{12}}{(1-z_1)(1-z_2)}$$

$$\frac{d^2\sigma_I^{31}}{dz_1\,dz_2} = -\frac{d^2\sigma_I^{32}}{dz_1\,dz_2} = \sigma^{(1)}\cdot\frac{1}{4\sqrt{2}}\cdot\frac{z_1^2\sin 2\theta_{13}+z_2^2\sin 2\theta_{23}}{(1-z_1)(1-z_2)} \qquad (2.5)$$

The angles θ_{12} and θ_{13} range from o to π, θ_{23} from π to 2π. $\left(\cos\theta_{ij} = 1 + \frac{2}{z_i z_j}(1 - z_i - z_j) \right)$.

$\sigma^{(1)} = \frac{2\alpha_s}{3\pi}\sigma^{(0)}$. We also have

$$\frac{d^2\sigma^{rs}_{TOT}}{dz_1\,dz_2} \equiv \frac{d^2(\sigma_U+\sigma_L)^{rs}}{dz_1\,dz_2} = \sigma^{(1)}\cdot\frac{z_1^2+z_2^2}{(1-z_1)(1-z_2)} \qquad (2.6)$$

for all possible r and s .

The cross sections σ_L, σ_T and σ_I are infrared finite, but σ_U (and σ_{TOT}) is not.

In order to avoid the infrared divergences in σ_U we used two different cutoff -procedures. First, we introduced a thrust-cutoff and second, we have calculated the two-particle inclusive cross section at a definite relative angle θ_{12} of the hadrons, thus avoiding the collinear divergences.

Let's first look at the thrust-cutoff case.

Including all the contributions from figure 2 we get

$$\frac{d^2\sigma_i^{h_1h_2}(x_1,x_2,T_0)}{dx_1\,dx_2} = \qquad (2.7)$$

$$\frac{1}{\sum_f e_f^2}\cdot\sum_q e_q^2\Bigg[\underbrace{\int_{x_1}^1\frac{dz_1}{z_1}\int_{x_2}^1\frac{dz_2}{z_2}\,\frac{d^2\sigma_i^{12}}{dz_1\,dz_2}\,D_q^{h_1}\!\left(\tfrac{x_1}{z_1}\right)D_{\bar q}^{h_2}\!\left(\tfrac{x_2}{z_2}\right)}_{\text{I+II}}\times$$

$$\times\,\theta(T_0-\max(z_1,z_2)) \;+$$

$$+\underbrace{\int_{x_1}^1\frac{dz_3}{z_3}\int_{x_2}^1\frac{dz_1}{z_1}\,\frac{d^2\sigma_i^{31}}{dz_1\,dz_3}\,D_q^{h_1}\!\left(\tfrac{x_1}{z_3}\right)D_{\bar q}^{h_2}\!\left(\tfrac{x_2}{z_1}\right)\theta(T_0-\max(z_1,z_3))}_{\text{I+III}}$$

$$+\underbrace{\int_{x_1}^1\frac{dz_2}{z_2}\int_{x_2}^1\frac{dz_3}{z_3}\,\frac{d^2\sigma_i^{23}}{dz_2\,dz_3}\,D_q^{h_1}\!\left(\tfrac{x_1}{z_2}\right)D_{\bar q}^{h_2}\!\left(\tfrac{x_2}{z_3}\right)\theta(T_0-\max(z_2,z_3))}_{\text{II+III}}$$

$$+\underbrace{\int_{x_1}^1\frac{dz_1}{z_1}\int_{x_2}^1\frac{dz_3}{z_3}\,\frac{d^2\sigma_i^{13}}{dz_1\,dz_3}\,D_q^{h_1}\!\left(\tfrac{x_1}{z_1}\right)D_{\bar q}^{h_2}\!\left(\tfrac{x_2}{z_3}\right)\theta(T_0-\max(z_1,z_3))}_{\text{I+III}}$$

$$+\underbrace{\int_{x_1}^1\frac{dz_2}{z_2}\int_{x_2}^1\frac{dz_1}{z_1}\,\frac{d^2\sigma_i^{21}}{dz_1\,dz_2}\,D_q^{h_1}\!\left(\tfrac{x_1}{z_2}\right)D_{\bar q}^{h_2}\!\left(\tfrac{x_2}{z_1}\right)\theta(T_0-\max(z_1,z_2))}_{\text{I+II}}$$

$$+\underbrace{\int_{x_1}^1\frac{dz_2}{z_2}\int_{x_2}^1\frac{dz_3}{z_3}\,\frac{d^2\sigma_i^{23}}{dz_2\,dz_3}\,D_{\bar q}^{h_1}\!\left(\tfrac{x_1}{z_2}\right)D_q^{h_2}\!\left(\tfrac{x_2}{z_3}\right)\theta(T_0-\max(z_2,z_3))}_{\text{II+III}}$$

$$+\underbrace{\int_{x_1}^1\frac{dz_3}{z_3}\int_{x_2}^1\frac{dz_1}{z_1}\,\frac{d^2\sigma_i^{31}}{dz_1\,dz_3}\,D_{\bar q}^{h_1}\!\left(\tfrac{x_1}{z_3}\right)D_q^{h_2}\!\left(\tfrac{x_2}{z_1}\right)\theta(T_0-\max(z_1,z_3))}_{\text{I+III}}$$

$$+\underbrace{\int_{x_1}^1\frac{dz_3}{z_3}\int_{x_2}^1\frac{dz_2}{z_2}\,\frac{d^2\sigma_i^{32}}{dz_2\,dz_3}\,D_{\bar q}^{h_1}\!\left(\tfrac{x_1}{z_3}\right)D_q^{h_2}\!\left(\tfrac{x_2}{z_2}\right)\theta(T_0-\max(z_2,z_3))}_{\text{II+III}}\Bigg]$$

where x_i (i=1,2) are the scaled hadron momenta, T_0 is the thrust-cutoff and the integration areas I,II and III[6] correspond to the cases where the quark, anti-quark and gluon, respectively, has the largest momentum. The sum is over quark species u,d,s,c and b only.

We now turn to consider the three-differential cross section

$$\frac{d^3\sigma_i^{h_1h_2}}{dx_1\,dx_2\,d\cos\theta_{12}}$$

where θ_{12} is the angle between the opposite hemisphere particles h_1 and h_2 ($\pi/2 < \theta_{12} < \pi$). The contributions of the figure 2 to this cross section are analogous to the thrust-cutoff case. We only have to replace the θ-function by a δ-function. For example, the first contribution is

$$\underbrace{\int_{x_1}^{1} \frac{dz_1}{z_1} \int_{x_2}^{1} \frac{dz_2}{z_2} \delta\left(1+\frac{2}{z_1 z_2}(1-z_1-z_2)-\cos\theta_{12}\right) \frac{d^2\sigma_i^{12}}{dz_1 dz_2} D_q^{h_1}\left(\frac{x_1}{z_1}\right) D_{\bar{q}}^{h_2}\left(\frac{x_2}{z_2}\right)}_{I} \quad (2.8)$$

Using the properties of δ-function we get

$$\int_{L(x_1,\cos\theta_{12})}^{U(x_1)} \frac{dz_1}{2-z_1(1-\cos\theta_{12})} \left[\frac{d^2\sigma_i^{12}}{dz_1 dz_2} D_q^{h_1}\left(\frac{x_1}{z_1}\right) D_{\bar{q}}^{h_2}\left(\frac{x_2}{z_2}\right)\right]_{z_2=z_2^\circ} \quad (2.9)$$

where

$$z_2^\circ = \frac{1-z_1}{1-\frac{z_1}{2}(1-\cos\theta_{12})} \quad . \quad (2.10)$$

The integration limits

$$L(x_1,\cos\theta_{12}) = \max\left[x_1, 2/3, \frac{1}{1-\cos\theta_{12}}, \frac{2}{1-\cos\theta_{12}} - \sqrt{\left(\frac{2}{1-\cos\theta_{12}}\right)^2 - \frac{2}{1-\cos\theta_{12}}}\right]$$

$$U(x_2) = \frac{1-x_2}{1-\frac{x_2}{2}(1-\cos\theta_{12})} \quad (2.11)$$

are obtained by demanding that the value z_2° must be reached inside the area I. All other contributions to the three-differential cross section are derived analogously. Therefore we do not list them here.

For the fragmentation we use a very simple model. We consider the case with only one quark, the u quark. The fragmentation function for this case is:

$$D_u^{h^\pm}(x) = 2\cdot\frac{(1-x)^2}{x} \quad , \quad D_u^{h^\circ}(x) = \frac{(1-x)^2}{x} \quad (2.12)$$

(where h^+, h^- and h° denote arbitrary positive, negative and neutral hadrons) with the favoured to unfavoured ratio:

$$\frac{D_u^{h^+}(x)}{D_u^{h^-}(x)} = \frac{1+x}{1-x} \quad (2.13)$$

This model is plausible only far above all mass thresholds, where the fragmentation functions for all quarks are supposed to be equal [3]:

$$D_u^{h^\pm}(x) = D_d^{h^\pm}(x) = D_s^{h^\pm}(x) = \ldots$$

However, the equalness of the ratio (2.13) is on a less firm basis.

For the gluon fragmentation function we considered two choices:

A.
$$D_g^{h^+}(x) = D_g^{h^-}(x) = D_g^{h^\circ}(x) = \frac{(1-x)^2}{x} \quad (2.14)$$

and

B. $$D_g^{h^+}(x) = D_g^{h^-}(x) = D_g^{h^\circ}(x) = 2\cdot\frac{1-x^2}{x} + 4\ln(x) \quad .$$

The first choice corresponds to the case, where the gluon fragments like a quark (more specifically: like the mean value of favoured and unfavoured quark fragmentation). The choice B corresponds to the situation where the gluon first decays into a quark-antiquark-pair, which then fragments into hadrons with the functions given in (2.12). In this case the neutral to charged normalization for the gluon fragmentation function is automatically the same as for the quark and drops out in all our calculations. This is not necessarily true for the case A in (2.14). Nevertheless we shall keep this normalization in both cases.

3. Results

We have normalized the cross sections

$$\frac{1}{\sigma^{(0)}} \cdot \frac{d^2\sigma_i^{h_1,h_2}(x_1,x_2,T_o)}{dx_1\,dx_2}$$ to the lowest order

charged particle production cross section

$$\frac{1}{\sigma^{(0)}}\cdot\frac{1}{2}\frac{d\sigma^{h^\pm}}{dx_1}\cdot\frac{1}{\sigma^{(0)}}\cdot\frac{1}{2}\frac{d\sigma^{h^\pm}}{dx_2} = D_U^{h^\pm}(x_1)\,D_U^{h^\pm}(x_2)\,. \qquad (3.1)$$

This ratio has been calculated for equal ($h_1 = h^+$, $h_2 = h^+$) and opposite charged ($h_1=h^+$, $h_2=h^-$) particles. The results for σ_U (with $T_o = 0.9$) are presented in table 1. The results for the cross sections σ_{TOT}, σ_L and σ_I, together with σ_U are shown in figure 3. (The symmetric part $x_2 > x_1$ has always been left out for clearness). We used for α_s the value 0.22 which corresponds to $\Lambda \approx 0.7$ GeV at $\sqrt{s} \approx 30$ GeV.

We see that the two choices of gluon fragmentation functions give roughly similar results for the low x region ($x \lesssim 0.3$), but are increasingly different for increasing x. Also with a smaller T_o as cut-off this difference increases more rapidly. The choice A gives consistently larger cross sections (except at extremely low x's) for σ_U and σ_L. The values of σ_I are always negative and small (of the order 10^{-4}-10^{-3}) and therefore are unlikely to be measurable.

Instead of absolute values of the cross sections we find it more interesting to present the ratio

$$r(x_1,x_2,T_o) = \frac{d^2\sigma_{TOT}^{h^+h^-}(x_1,x_2,T_o)}{d^2\sigma_{TOT}^{h^+h^+}(x_1,x_2,T_o)} \qquad (3.2)$$

and its dependence on x and T_o.

This ratio is shown in figures 4 for three representative values of x. Also shown is the corresponding ratio from the

lowest order term:

$$r^{(0)}(x_1,x_2) = \frac{D_U^{h^+}(x_1)\,D_U^{h^+}(x_2) + D_U^{h^-}(x_1)\,D_U^{h^-}(x_2)}{D_U^{h^+}(x_1)\,D_U^{h^-}(x_2) + D_U^{h^-}(x_1)\,D_U^{h^+}(x_2)} \qquad (3.3)$$

At large x the deviation from the lowest order contribution is quite remarkable. For low x the ratio (3.2) is almost constant with T_o and for the choice B it is only somewhat higher. For the larger x the difference between the two choices A and B is quite drastic. The curve for B is much higher and is decreasing with increasing T_o while that for A is increasing. This can be understood to be due to the different behaviour of the two gluon fragmentation functions at $x \to 1$ (A: $\sim(1-x)^2$, B: $\sim(1-x)^3$). Perhaps this might be used for a possible check of the behaviour of the gluon fragmention for $x \to 1$.

The three-differential cross section

$$\frac{1}{\sigma^{(0)}}\cdot\frac{d^3\sigma_i^{h_1,h_2}}{dx_1\,dx_2\,d\cos\theta_{12}} \qquad (3.4)$$

(normalized to (3.1)) for σ_{TOT}, σ_L and σ_I are plotted in figures 5 for opposite charged particles for some specific x-values. For clearness, also the ratio of $d^3\sigma_{TOT}^{h^+h^-}/dx_1dx_2\,d\cos\theta_{12}$ for the two different gluon fragmentation functions is presented in figure 6. The tendency is clear but the effect remains small.

As the next point we consider the ratio

$$\tilde{r}(x_1,x_2,\theta_{12}) = \frac{d^3\sigma_{TOT}^{h^+h^-}(x_1,x_2,\cos\theta_{12})}{d^3\sigma_{TOT}^{h^+h^+}(x_1,x_2,\cos\theta_{12})} \qquad (3.5)$$

which is shown for certain x-values in figure 7. The behaviour of $\tilde{r}$ with θ_{12} is analogous to that of r as a function of T_o (at the same x), because a particular thrust-value T corresponds to a certain average angle $\langle\theta_{12}(T)\rangle$, which increases with increasing T. As a result we find that also the ratio $\tilde{r}$ for the three - differential cross sections is sensitive at moderate and large x-values to the gluon fragmentation function near x=1.

As the final point we compare our model with experimental results from the Pluto collaboration [9] on the correlation of charged particles in opposite hemispheres (fig.8). We see that our model fits the data best for $\theta_a = \pi - \theta_{12} \gg 0$, where the effect of hard gluon bremsstrahlung is supposed to be cleanest. Because of the three particle kinematics and our neglect of p_T-spread of fragmentation the model gives zero for $\theta_a > 90^o$. First-order perturbation theory is certainly not expected to explain the region $\theta_{12} \approx 0$, where multiple gluon emission [10] seems to be crucial. Finally, we point out that to get more reliable results at the (non-asymptotic) c.m.-energy of 30 GeV we should certainly take into account the non-perturbative p_T-spread of quark and gluon fragmentation.

Acknowledgment

I would like to thank G.Kramer for suggesting this work and critically reading the manuscript an G.Schierholz for helpful discussions. I am indebted to the Deutscher Akademischer Austauschdienst for support.

References

1) J.Bechteler and L.Stodolsky, Phys.Lett. 84B (1979),455
C.Peterson, Z.Physik C3 (1980), 271

2) Tasso collaboration, R.Brandelik et al., Phys.Lett. 86B (1979), 243
Mark-J collaboration, D.P.Barber et al., Phys.Rev.Lett.43 (1979), 830
Pluto collaboration, Ch.Berger et al., Phys.Lett. 86B (1979), 418

3) G.Schierholz and J.Willrodt, Z.Physik C3 (1979),125

4) J.Ellis, M.K.Gaillard and G.G.Ross, Nucl.Phys. B111 (1976), 253

5) G.Kramer and G.Schierholz, Phys.Lett.82B (1979),108
P.Hoyer et al., Nucl.Phys. B 161 (1979), 349

6) G.Kramer, G.Schierholz and J.Willrodt, Phys.Lett.79B (1978), 249
Err.Ibid. 80B (1979), 433

7) S.Y.Pi et al., Phys.Rev.Lett. 41 (1978), 142

8) A.Ali, J.G.Körner, G.Kramer and J.Willrodt, DESY report 79/63 (1979) and Nucl.Phys. (to be published)
A.Ali, E.Pietarinen, G.Kramer and J.Willrodt, DESY report 79/86 and Phys.Lett. (to be published).

9) Pluto collaboration, Ch.Berger et al., Phys.Lett. 90B (1980), 312

10) Yu.L.Dokhitzer, D.I.D'yakonov, S.I.Troyan, Phys.Lett. 78B (1978), 290

Tables and figures

Table 1: The normalized two-particle distributions for σ_U are presented as follows. Above the dotted line for any x-values is the result for equally charged particles using the choice (2.14.A) (higher number) and (2.14.B) (lower number). Under the dotted line are the numbers for opposite charged particles in the same order. The thrust-cutoff is $T_0 = 0.9$.

Fig.1 a): Lowest order diagram for hadron production in e^+e^--annihilation.
b) and c): Second order QCD-diagrams for three-jet production in e^+e^--annihilation.

Fig.2 The parton content of the two-particle opposite hemisphere inclusive cross sections with the quark (I), antiquark (II) and gluon (III) momentum, respectively, defining the thrust axis.

Fig.3 The normalized two-particle inclusive total cross section for opposite charged particles with $T_o = 0.9$ using the choice (2.14.A).

(a): σ_{TOT} The highest value is 0.1343
(b): σ_U — " — 0.113
(c): σ_L — " — 0.0213
(d): σ_I The lowest value is $-2.37.10^{-3}$.

Fig.4 The ratio r as a function of T_o. The upper (dashed) curves correspond to the choice (2.14.B), the lower to (2.14.A).
The dash-dotted constant curve is the value of $r^\circ(x_1,x_2)$ (see eq.(3.3))

(a): x_1=0.3, x_2=0.2
(b): x_1=x_2=0.5
(c): x_1=0.7, x_2=0.3

Fig.5 The normalized two-particle distributions at a definite angle for opposite charged particles and for various x's. The case (2.14.A) is presented.

(a): σ_{TOT}
(b): σ_L
(c): σ_I

Fig.6 The ratio $d^3\sigma_{TOT}^{h^+h^-}$ (choice A) / $d^3\sigma_{TOT}^{h^+h^-}$ (choice B) for some x-values as a function of θ_{12}. The straight line is for x_1=0.3, x_2=0.2, the dashed for x_1=x_2=0.5 and the dashed-dotted for x_1=0.8, x_2=0.4.

Fig.7 The ratio $\tilde{r}(x_1, x_2, \theta_{12})$ is presented for σ_{TOT} as a function of θ_{12}.
The upper (dashed) curves correspond to the choice (2.14.B), the lower to (2.14A).

(a): x_1= 0.3, x_2=0.2
(b): x_1= x_2 = 0.5
(c): x_1= 0.8, x_2=0.4

Fig.8 The data from the Pluto group (see ref.9, fig.1.d) on the correlation of charged particles in opposite hemispheres is presented together with our theoretical curve. (The cm. energy is between 27.6 and 31.6 GeV for the data, 30 GeV for the curve).

	o.1	o.2	o.3	o.4	o.5	o.6	o.7	o.8
o.1	o.111 o.112	o.o964 o.o917	o.o822 o.o762	o.o683 o.o625	o.o542 o.o492	o.o392 o.o355	o.o232 o.o2o9	o.oo751 o.oo674
	o.113 o.115	o.1oo o.o955	o.o871 o.o811	o.o738 o.o68o	o.o596 o.o547	o.o439 o.o4o2	o.o264 o.o241	o.oo871 o.oo794
o.2		o.o792 o.o687	o.o66o o.o552	o.o536 o.o438	o.o414 o.o334	o.o291 o.o232	o.o166 o.o131	o.oo516 o.oo4o6
		o.o857 o.o753	o.o745 o.o636	o.o63o o.o532	o.o5o7 o.o427	o.o371 o.o312	o.o221 o.o186	o.oo713 o.oo6o4
o.3			o.o519 o.o416	o.o41o o.o321	o.o3o8 o.o237	o.o21o o.o159	o.o116 o.oo873	o.oo348 o.oo263
			o.o626 o.o524	o.o529 o.o439	o.o425 o.o353	o.o3o9 o.o258	o.o182 o.o154	o.oo586 o.oo5o1
o.4				o.o3o8 o.o235	o.o225 o.o168	o.o149 o.o11o	o.oo796 o.oo582	o.oo233 o.oo17o
				o.o436 o.o364	o.o35o o.o293	o.o254 o.o215	o.o15o o.o129	o.oo485 o.oo422
o.5					o.o156 o.o115	o.o1oo o.oo725	o.oo522 o.oo371	o.oo149 o.oo1o4
					o.o276 o.o235	o.o2o1 o.o173	o.o119 o.o1o4	o.oo387 o.oo342
o.6						o.oo616 o.oo436	o.oo311 o.oo213	o.oo085 o.oo057
						o.o145 o.o127	o.oo864 o.oo766	o.oo283 o.oo254
o.7							o.oo149 o.oo097	o.ooo39 o.ooo24
							o.oo513 o.oo462	o.oo169 o.oo153
o.8								o.ooooo9 o.ooooo5
								o.oo055 o.oo051

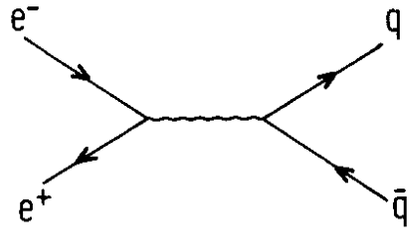

(a)

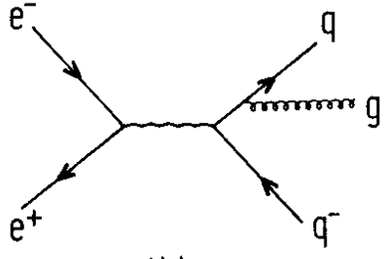

(b)

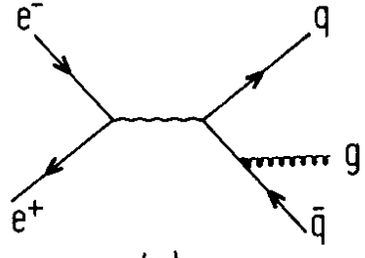

(c)

Fig.1

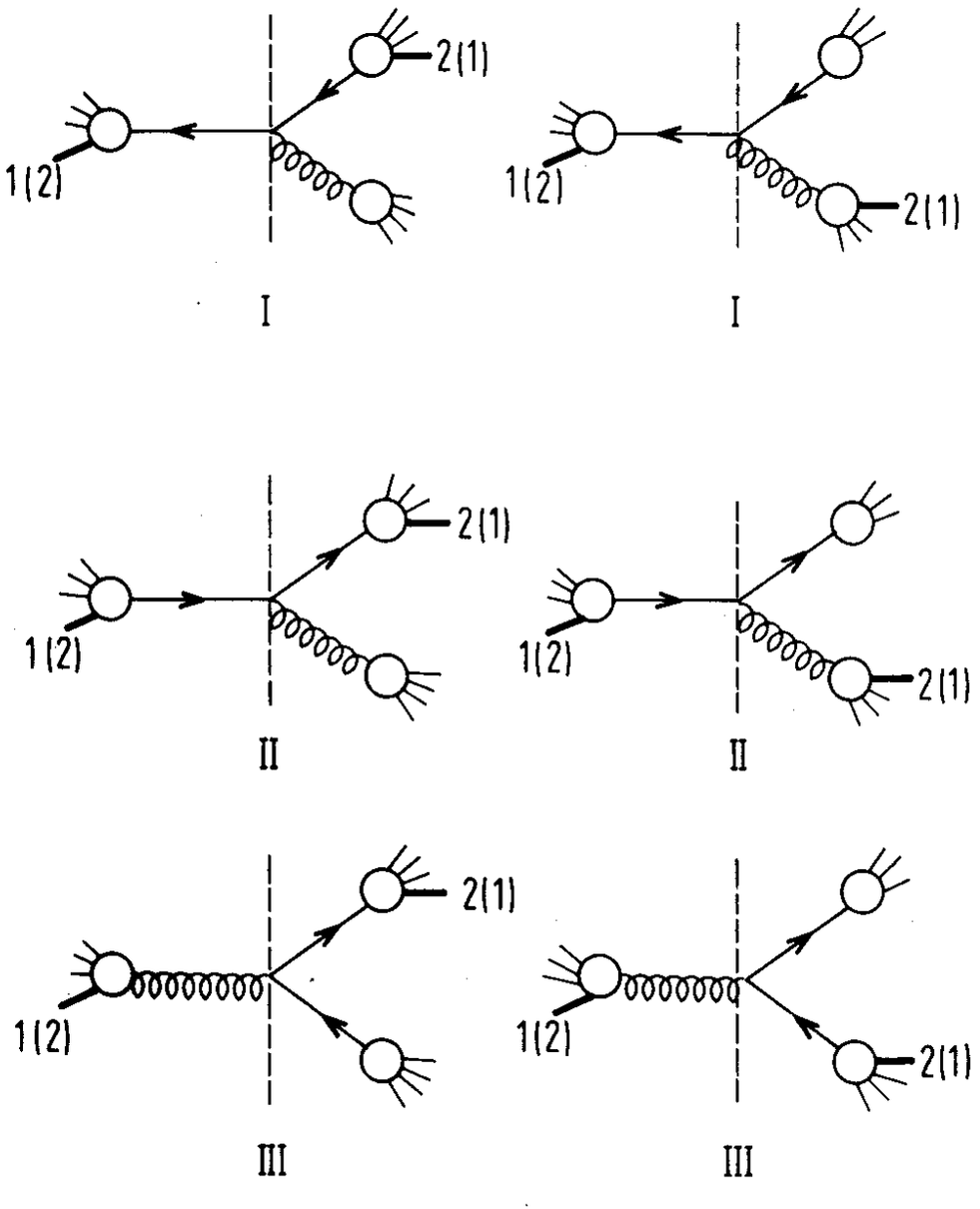
2(1)
1(2)
I
1(2)
2(1)
I
2(1)
1(2)
II
1(2)
2(1)
II
2(1)
1(2)
III
1(2)
2(1)
III

Fig. 2

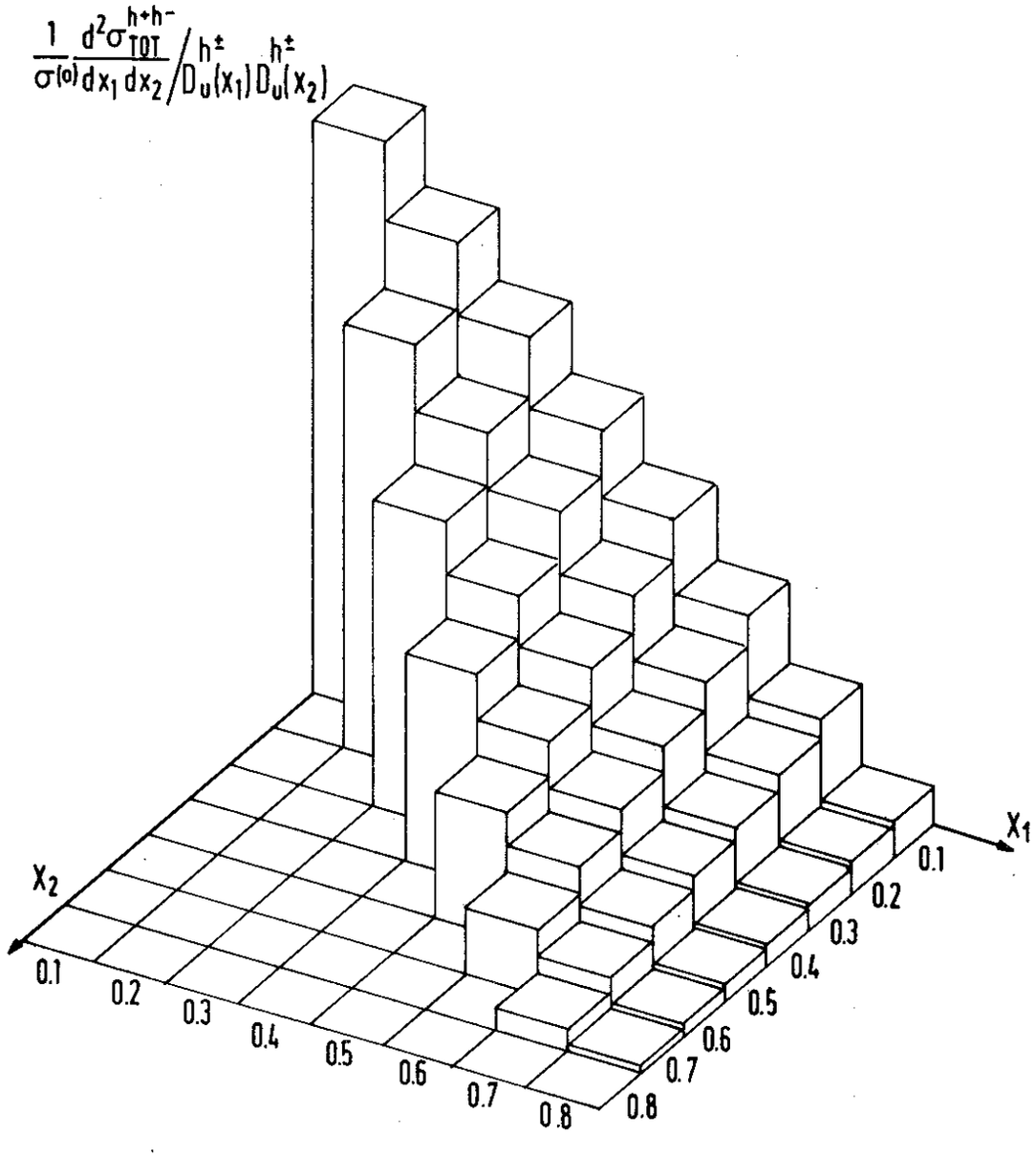
$\frac{1}{\sigma^{(0)}}\frac{d^2\sigma_{TOT}^{h^+h^-}}{dx_1\,dx_2}\Big/D_u^{h^\pm}(x_1)\,D_u^{h^\pm}(x_2)$
X_2
X_1
0.1
0.2
0.3
0.4
0.5
0.6
0.7
0.8

Fig.3a

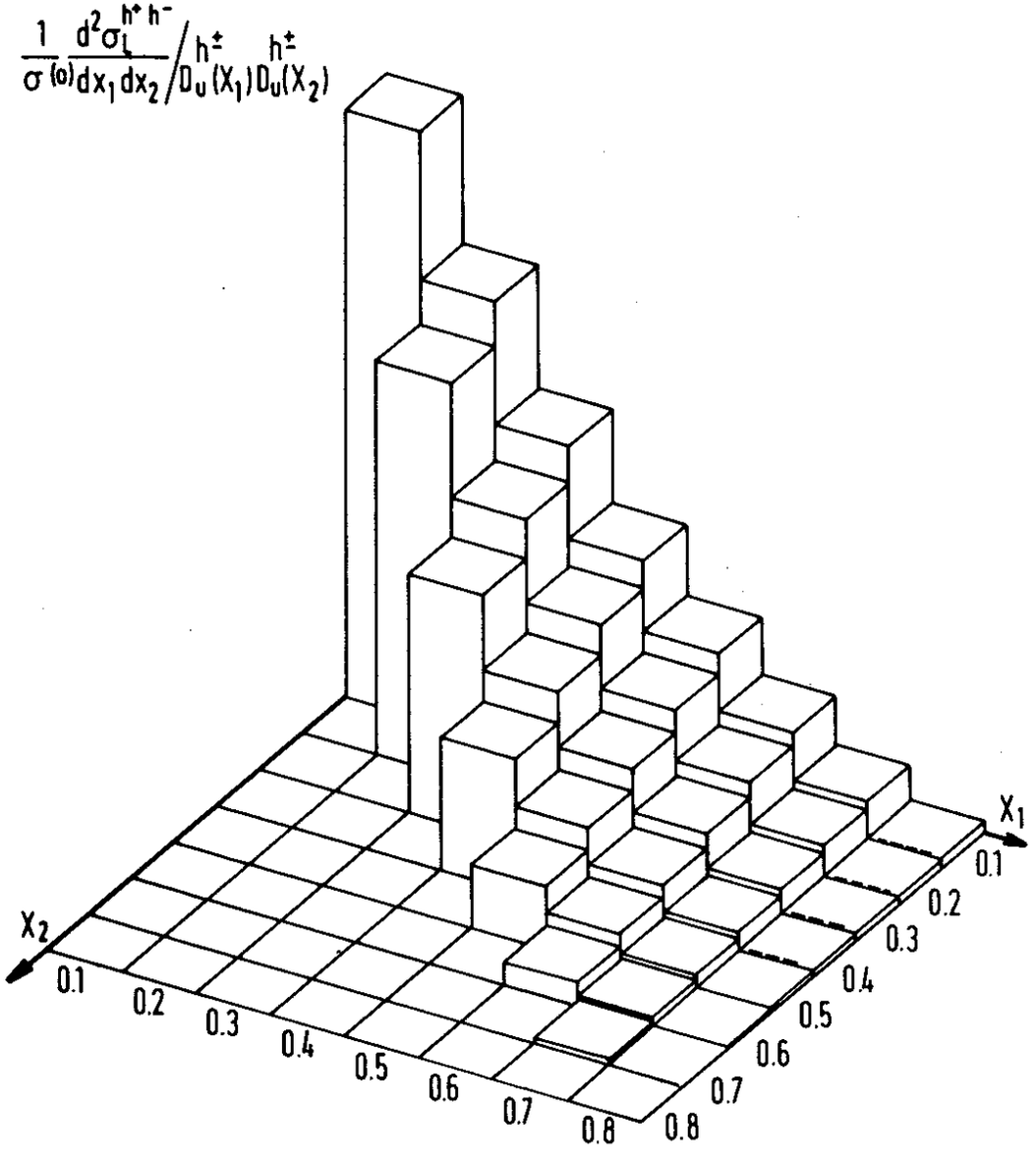
$\frac{1}{\sigma^{(0)}}\frac{d^2\sigma_L^{h^+h^-}}{dx_1\,dx_2}\Big/D_u^{h^\pm}(X_1)D_u^{h^\pm}(X_2)$
X_1
X_2
0.1
0.2
0.3
0.4
0.5
0.6
0.7
0.8

Fig. 3 c

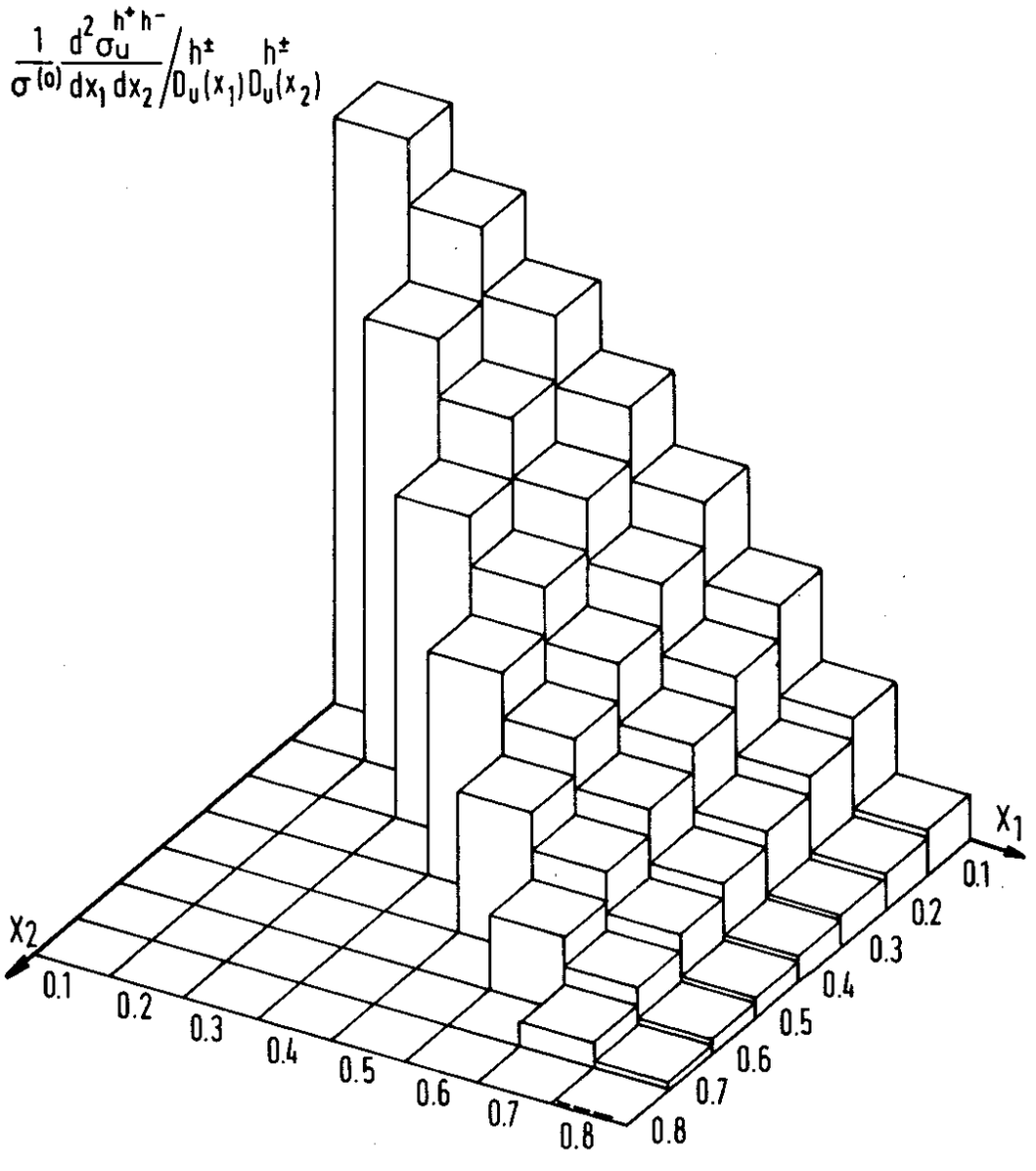
$\frac{1}{\sigma^{(0)}}\frac{d^2\sigma_U^{h^+h^-}}{dx_1\,dx_2}\Big/D_u^{h^\pm}(x_1)D_u^{h^\pm}(x_2)$
X_1
X_2
0.1
0.2
0.3
0.4
0.5
0.6
0.7
0.8

Fig. 3 b

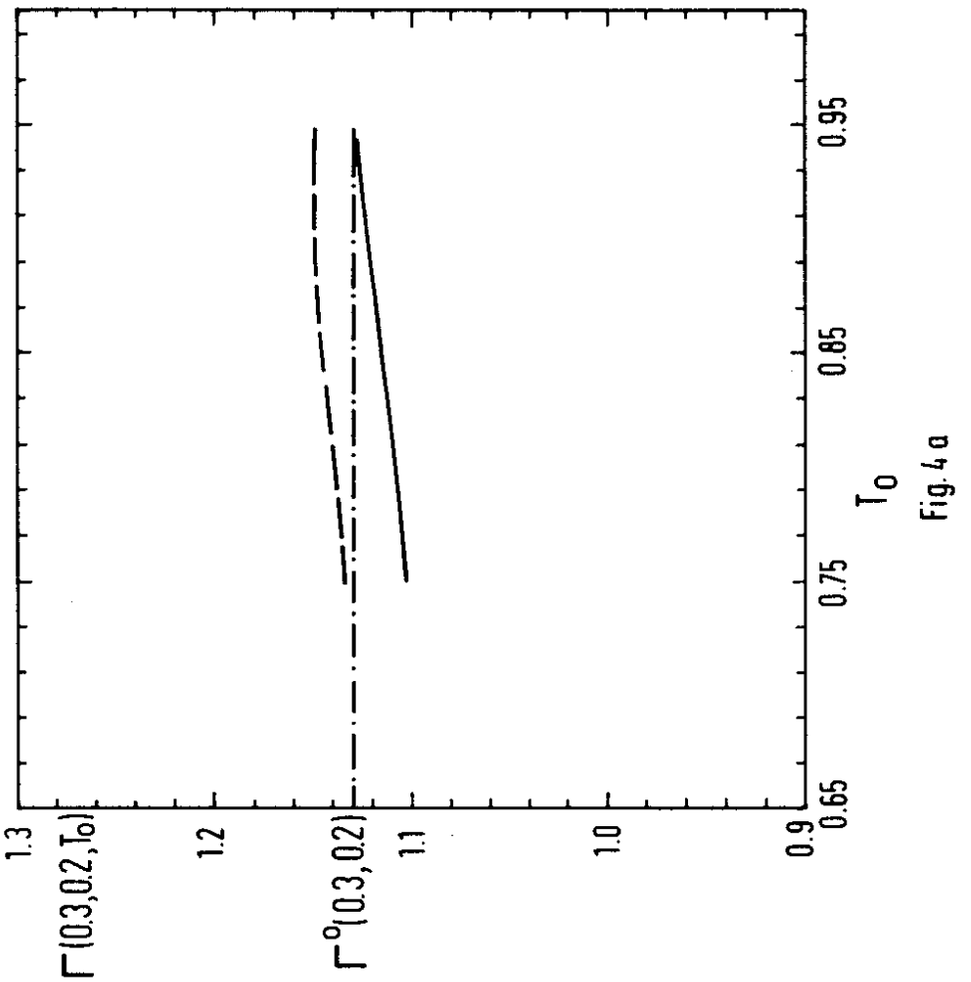
1.3
1.2
1.1
1.0
0.9
0.95
0.85
0.75
0.65
T_0
$\Gamma(0.3,0.2,T_0)$
$\Gamma^0(0.3,0.2)$

Fig. 4 a

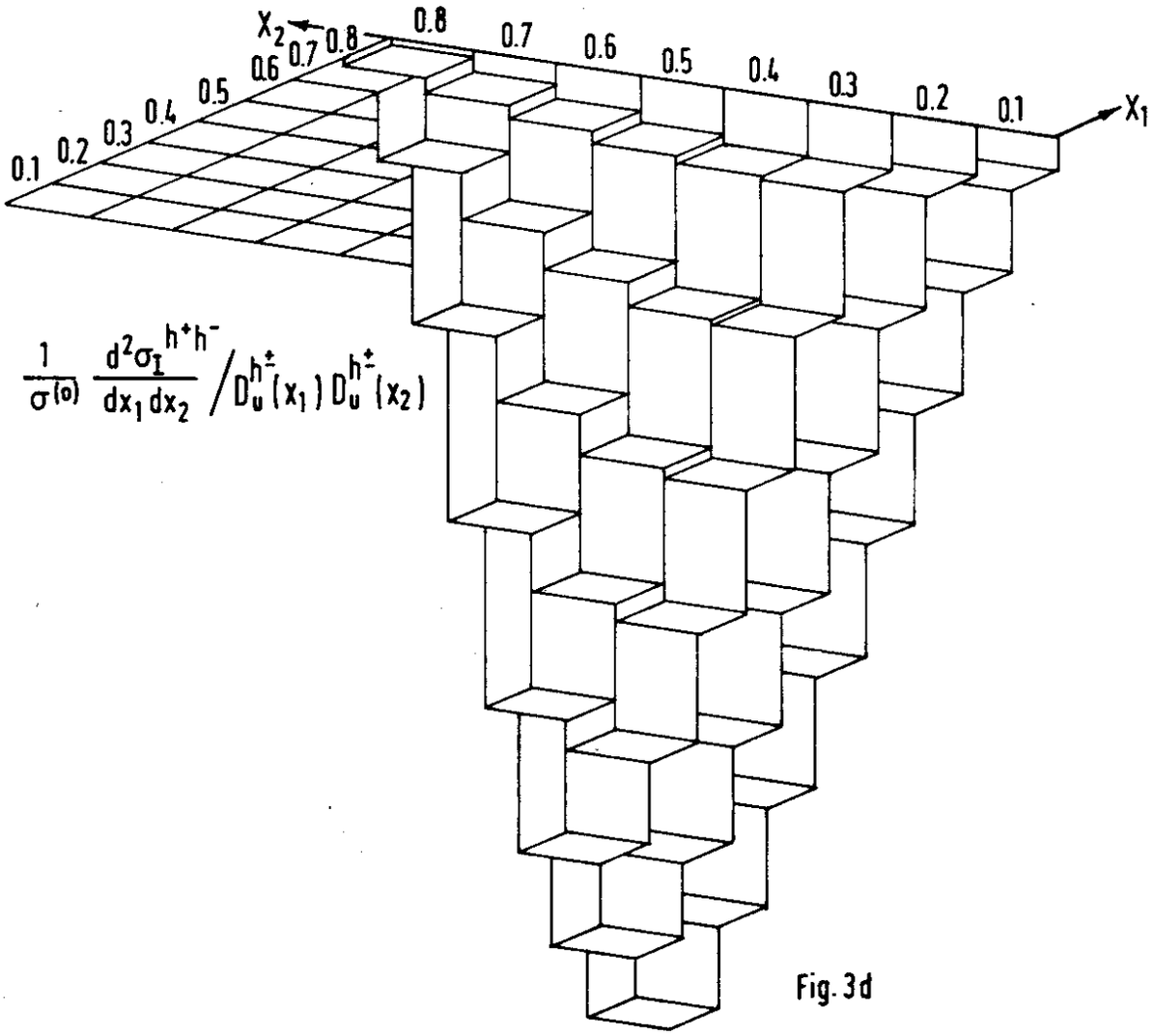
X_2
X_1
0.1
0.2
0.3
0.4
0.5
0.6
0.7
0.8
$\frac{1}{\sigma^{(0)}} \frac{d^2\sigma_I^{h^+h^-}}{dx_1\,dx_2} / D_u^{h^\pm}(x_1)\, D_u^{h^\pm}(x_2)$

Fig. 3 d

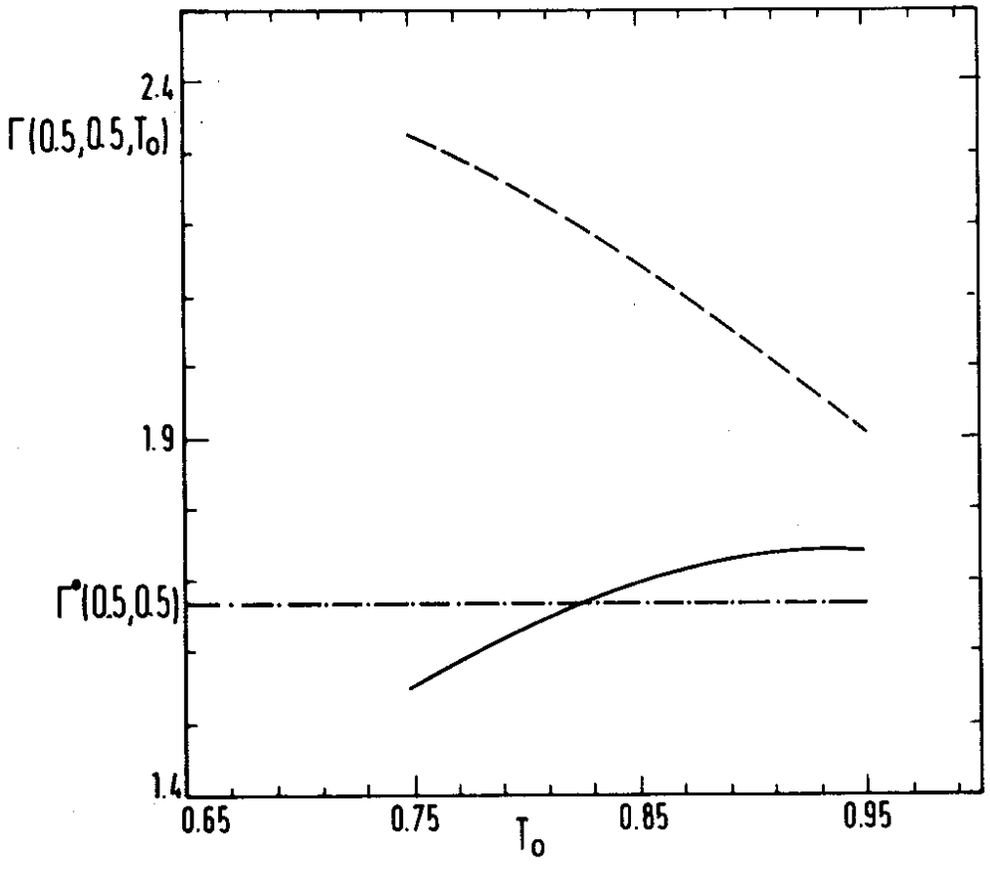
2.4
Γ(0.5,0.5,T0)
1.9
Γ°(0.5,0.5)
1.4
0.65
0.75
T0
0.85
0.95

Fig. 4 b

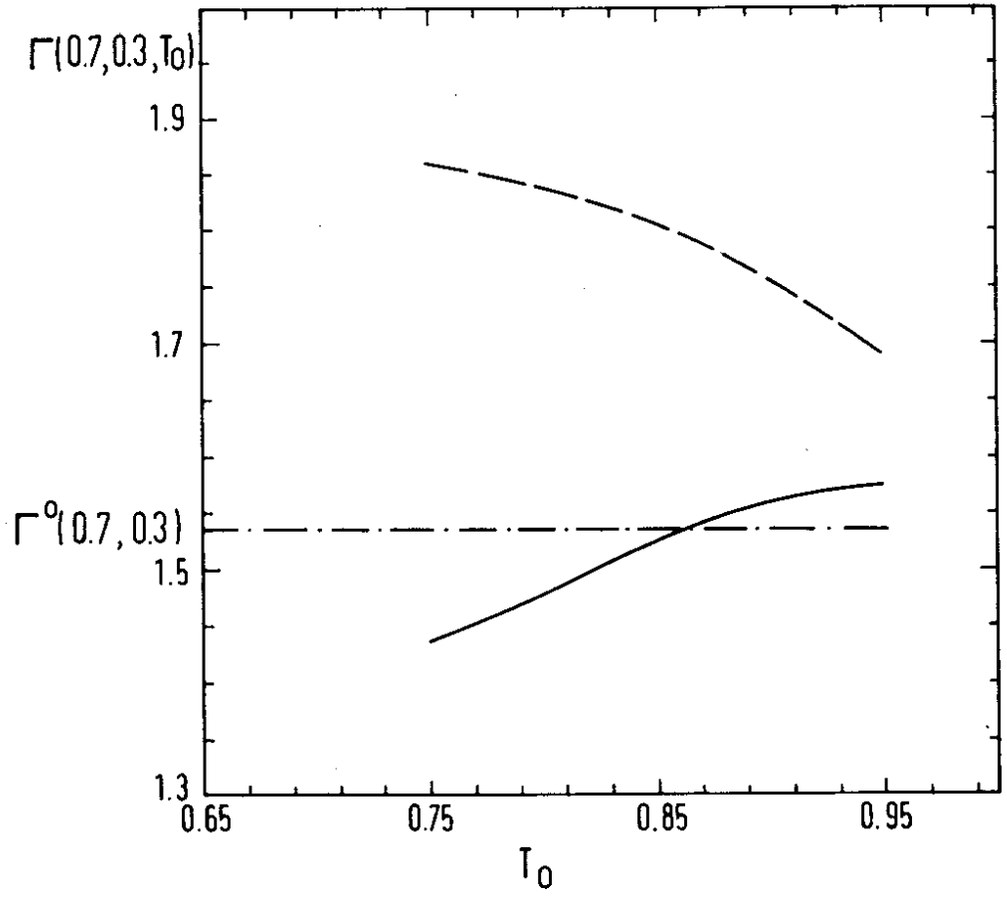
Γ(0.7,0.3,T0)
1.9
1.7
Γ°(0.7,0.3)
1.5
1.3
0.65
0.75
0.85
0.95
T0

Fig. 4 c

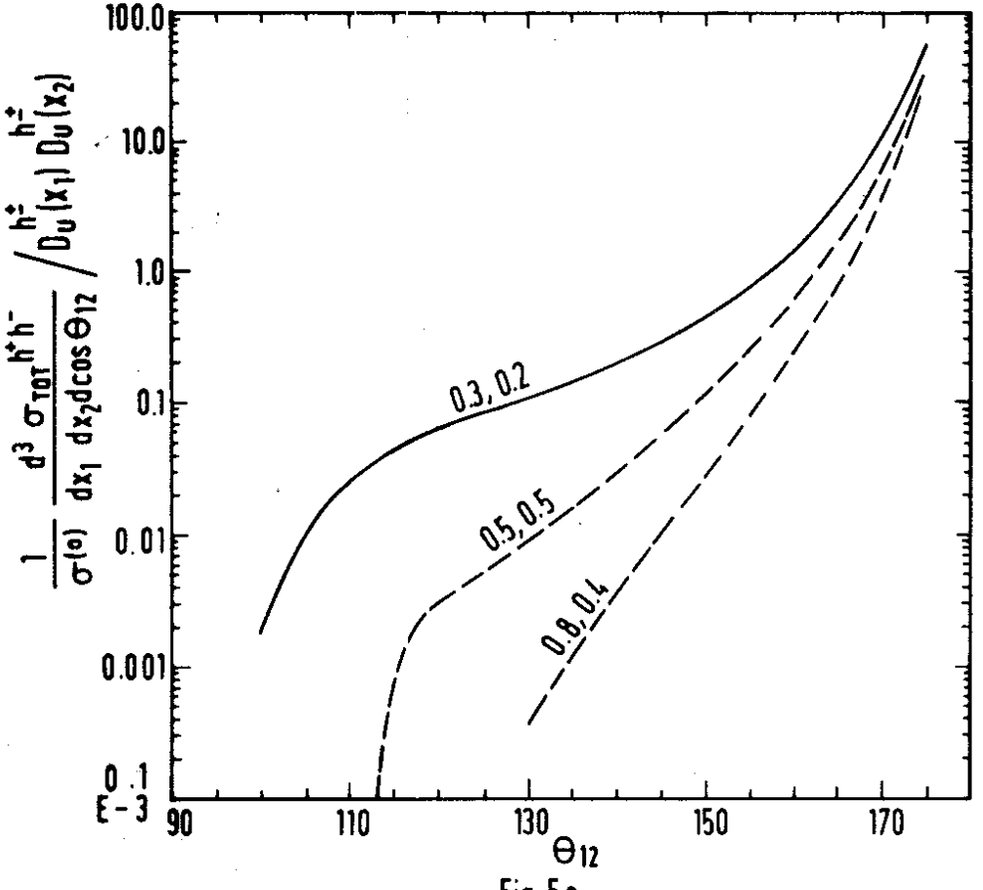
100.0
10.0
1.0
0.1
0.01
0.001
0.1
E-3
90
110
130
150
170
Θ_{12}
$\frac{1}{\sigma^{(0)}} \frac{d^3 \sigma_{TOT}^{h^+h^-}}{dx_1\, dx_2 d\cos\Theta_{12}} \Big/ D_U^{h_1^+}(x_1)\, D_U^{h_2^-}(x_2)$
0.3, 0.2
0.5, 0.5
0.8, 0.4

Fig. 5a

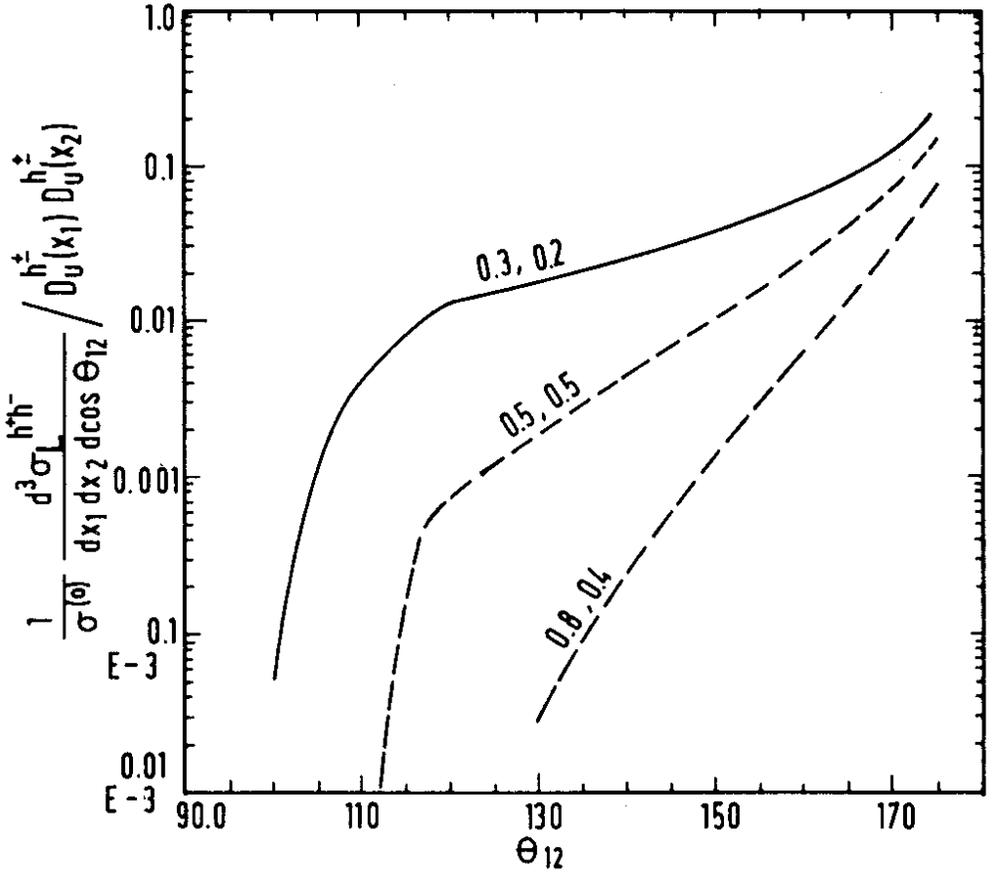
1.0
0.1
0.01
0.001
0.1
E-3
0.01
E-3
90.0
110
130
150
170
Θ_{12}
$\frac{1}{\sigma^{(0)}} \frac{d^3 \sigma_L^{h^+h^-}}{dx_1\, dx_2 d\cos\Theta_{12}} \Big/ D_U^{h_1^+}(x_1)\, D_U^{h_2^-}(x_2)$
0.3, 0.2
0.5, 0.5
0.8, 0.4

Fig. 5b

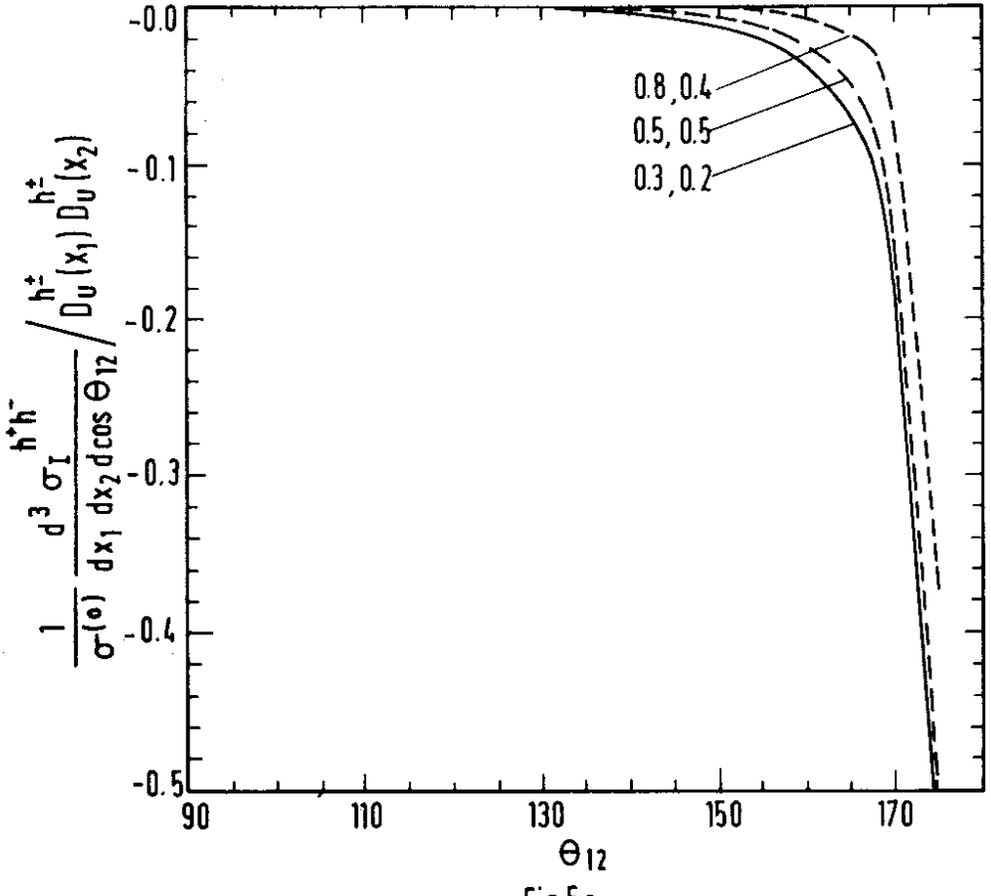
$\frac{1}{\sigma^{(0)}} \frac{d^3\sigma_I^{h^+h^-}}{dx_1\, dx_2\, d\cos\Theta_{12}} \Big/ D_U^{h^+}(x_1)\, D_U^{h^-}(x_2)$
-0.0
-0.1
-0.2
-0.3
-0.4
-0.5
0.8, 0.4
0.5, 0.5
0.3, 0.2
90
110
130
150
170
Θ_{12}

Fig. 5c

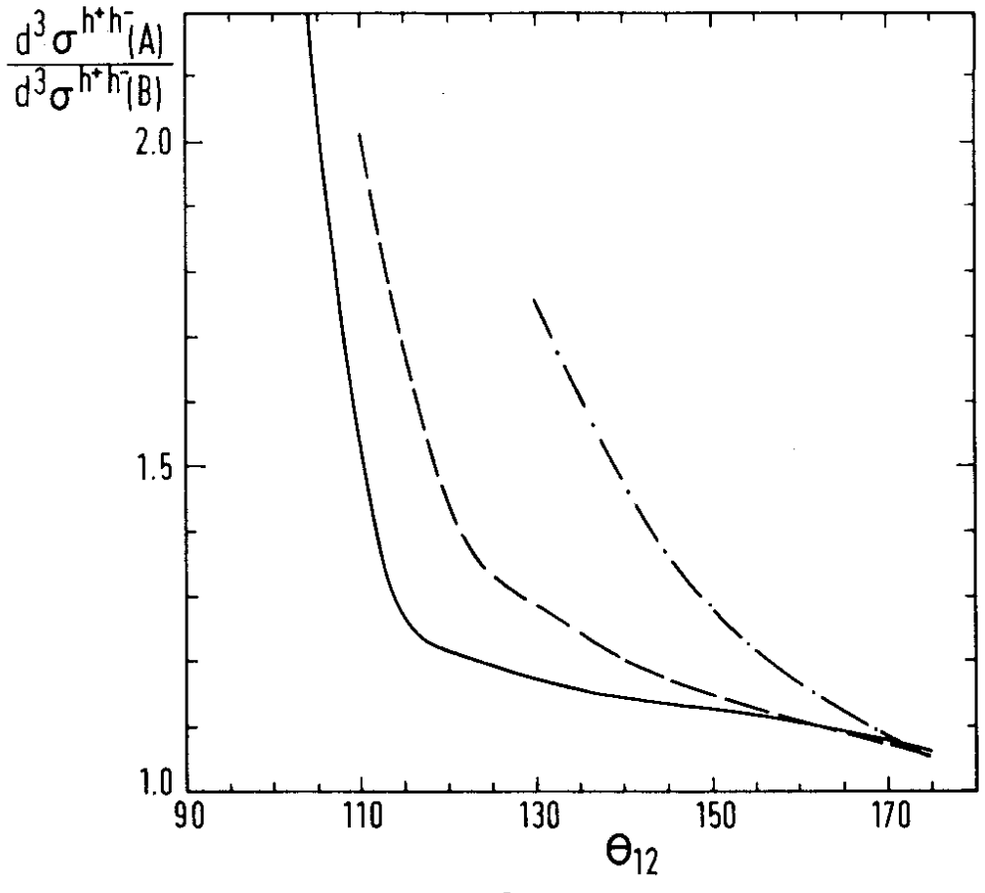
$\frac{d^3\sigma^{h^+h^-}(A)}{d^3\sigma^{h^+h^-}(B)}$
2.0
1.5
1.0
90
110
130
150
170
Θ_{12}

Fig. 6

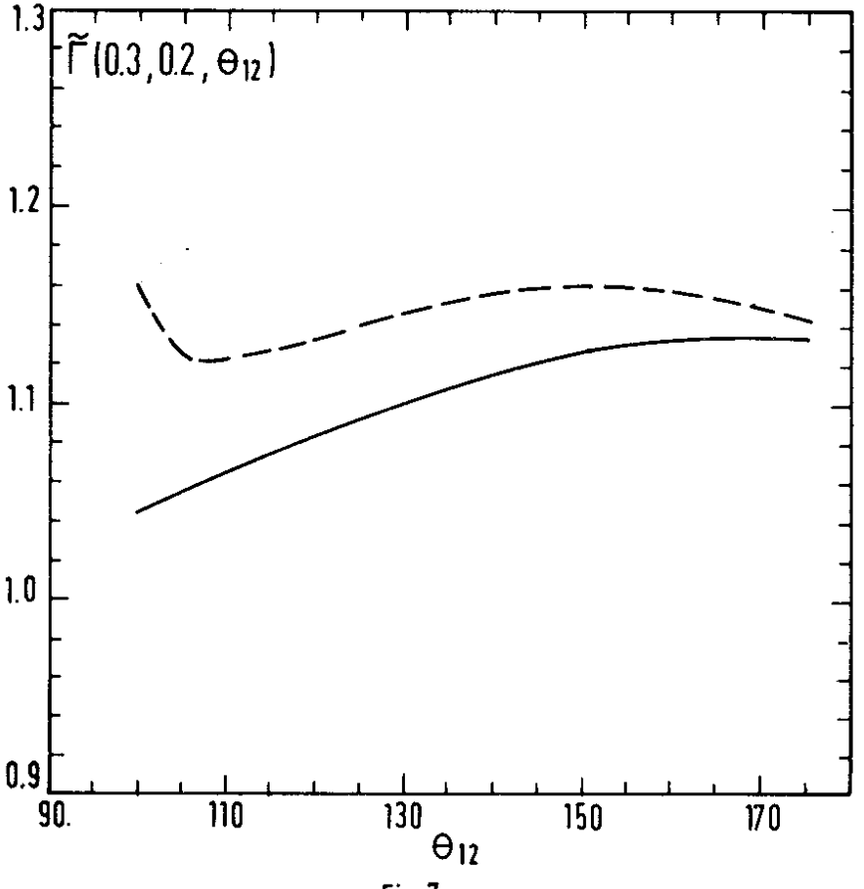
$\tilde{\Gamma}(0.3, 0.2, \theta_{12})$
1.3
1.2
1.1
1.0
0.9
90.
110
130
150
170
θ_{12}

Fig.7a

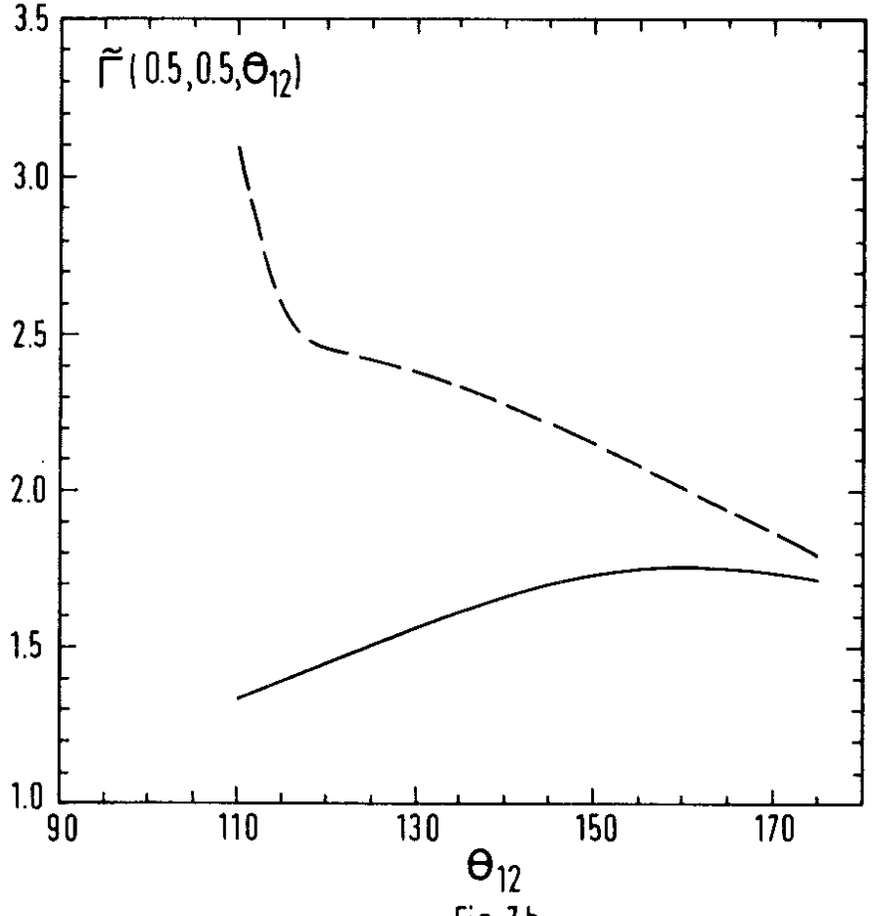
$\tilde{\Gamma}(0.5, 0.5, \theta_{12})$
3.5
3.0
2.5
2.0
1.5
1.0
90
110
130
150
170
θ_{12}

Fig.7b

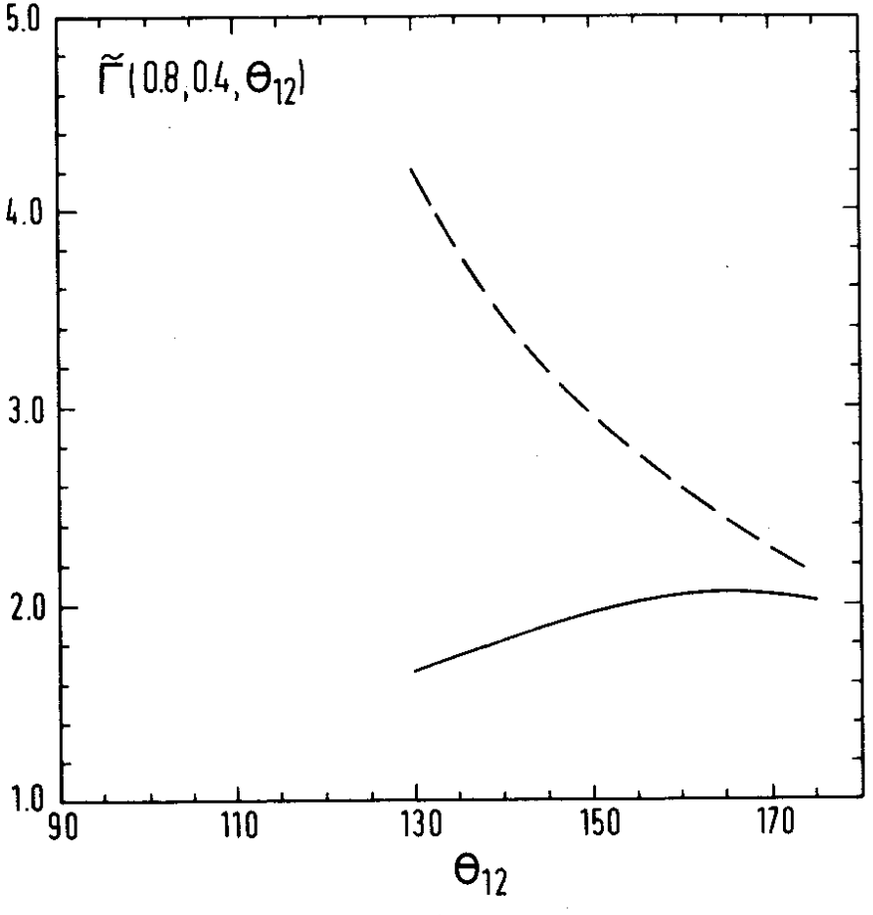
5.0
4.0
3.0
2.0
1.0
$\tilde{\Gamma}(0.8, 0.4, \Theta_{12})$
90
110
130
150
170
Θ_{12}

Fig. 7c

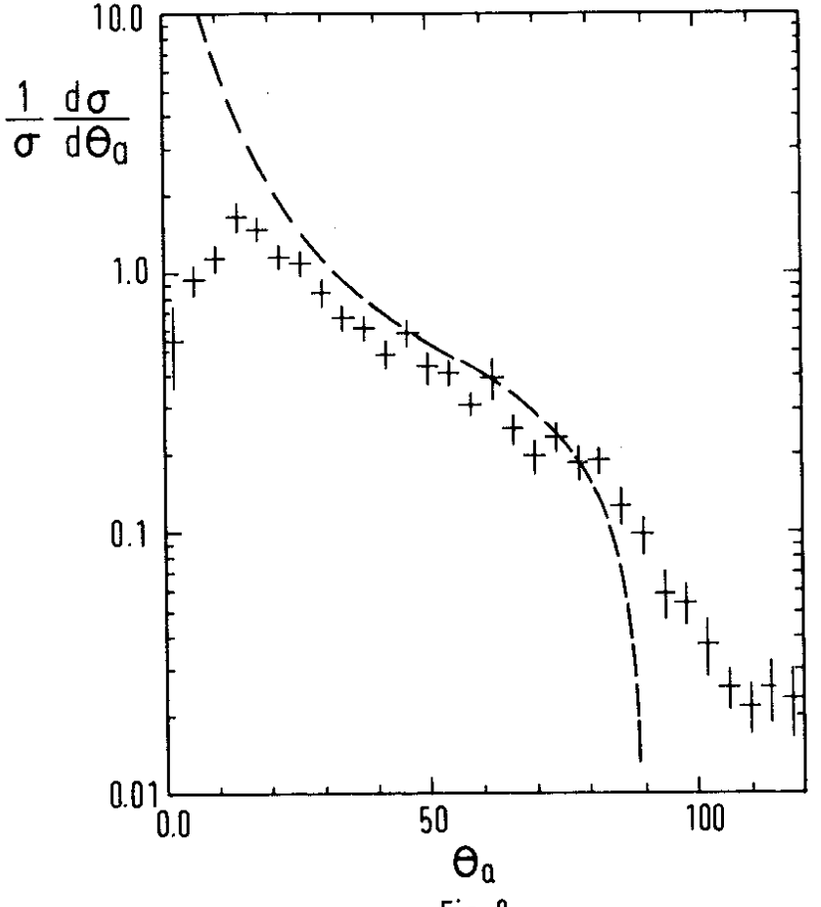
10.0
1.0
0.1
0.01
$\frac{1}{\sigma}\frac{d\sigma}{d\Theta_a}$
0.0
50
100
Θ_a

Fig. 8